VNUHCM Journal of Science and Technology Development 2026, 29(1):3919-3925

Open Access Full Text Article

Research Article

Thermoelectric properties of Ga-doped ZnO produced via a green synthesis method

Nhi Hoang Nguyen[1,2,3], Uyen Tu Thi Doan[1,2], Dung Van Hoang[1,2], Truong Huu Nguyen[1,2], Trieu Quang Vo[1,2], Vinh Cao Tran[1,2,3], Anh Tuan Thanh Pham[1,2,*]

[1]*Laboratory of Advanced Materials, University of Science, Ho Chi Minh City, Vietnam*

[2]*Vietnam National University, Ho Chi Minh City, Ho Chi Minh City, Vietnam*

[3]*Advanced Materials Technology Institute Vietnam National University Ho Chi Minh City, Ho Chi Minh City, Vietnam*

Correspondence

Anh Tuan Thanh Pham, Laboratory of Advanced Materials, University of Science, Ho Chi Minh City, Vietnam

Vietnam National University, Ho Chi Minh City, Ho Chi Minh City, Vietnam

Email: pttanh@hcmus.edu.vn

History

- Received: 06-08-2025
- Revised: 13-10-2025
- Accepted: 22-10-2025
- Published Online: 09-01-2026

DOI :

https://doi.org/10.32508/stdj.v29i1.4562

ABSTRACT

$Ga_xZn_{1-x}O$ (x = 0, 0.01, and 0.02) nanoparticles were synthesized via a simple, low-cost, and eco-friendly method using orange peel extract as a stabilizing agent. Research on such green synthesis approaches for Ga-doped ZnO remains limited. The crystal structure and thermoelectric properties of the samples were investigated. Gallium (Ga) doping improved the crystal structure and temperature-dependent electrical conductivity of ZnO. In particular, the Ga-doped ZnO sample with 2 at.% Ga (GZO-2) exhibited an electrical conductivity nearly 30 times higher than that of undoped ZnO at 1068 K. Furthermore, the power factor of this sample reached approximately 56 $\mu W/mK^2$ at 1068 K, nearly twofold higher than that of undoped ZnO. Additionally, the reduced grain size enhanced grain boundary scattering, markedly decreasing thermal conductivity. Therefore, GZO-2 exhibited the highest figure of merit, approximately 2.5 times higher than that of undoped ZnO. These results highlight the novelty of using agricultural-waste-derived orange peel extract in green synthesis and demonstrate the effectiveness of Ga doping in enhancing the thermoelectric performance of ZnO through microstructural modification.

Key words: thermoelectrics, Ga-doped ZnO, green synthesis, power factor

INTRODUCTION

Zinc oxide (ZnO) is a typical n-type semiconductor, characterized by its non-toxicity and natural abundance. ZnO exhibits high carrier mobility and thermal stability. Although its properties make it a promising candidate for thermoelectric applications, ZnO still has limitations, primarily its low electrical conductivity, which is due to a low carrier concentration, and high thermal conductivity, which results from its simple crystal structure and strong atomic bonding[1]. Various strategies have been proposed to overcome these drawbacks, including elemental doping and the synthesis of nanostructured materials to enhance the thermoelectric properties of ZnO. Herein, gallium (Ga) was chosen as the dopant element for ZnO. Ga has a trivalent oxidation state; thus, when Ga^{3+} substitutes for Zn^{2+} in the ZnO lattice, it contributes additional free electrons, enhancing the electrical conductivity. Moreover, the ionic radii of Ga^{3+} (0.062 nm) and Zn^{2+} (0.074 nm) are similar, making Ga a suitable dopant for ZnO [2]. Several studies have investigated the thermoelectric properties of bulk Ga-doped ZnO ceramics. For example, Jung et al. reported that Ga incorporation enhanced the electrical conductivity of ZnO[2]. However, the highest power factor (PF = $S^2\sigma$, where S and σ are the Seebeck coefficient and electrical conductivity, respectively) remained modest, ~1250 $\mu W/mK^2$ at 1273 K for the $Zn_{0.985}Ga_{0.015}O$ bulk sample. In a subsequent work, Jung et al. improved the thermoelectric performance by optimizing the synthesis conditions, with the highest PF being approximately 918 $\mu W/mK^2$ at 1050 K for the $Zn_{0.98}Ga_{0.02}O$ pellet[3]. In addition, Guilmeau et al. investigated Ga-doped ZnO prepared at various Ga concentrations[4]. The $Zn_{1-x}Ga_xO$ sample with x = 0.005 exhibited the highest PF (~700 mW/mK^2). However, Guilmeau et al. noted that when the Ga content exceeded x = 0.005, tended to decrease, likely due to the formation of structural defects that introduced electron scattering and hindered charge transport. These findings reveal the potential of Ga doping in enhancing the thermoelectric properties of ZnO and demonstrate the importance of optimizing the Ga concentration to achieve the highest performance. Therefore, here, $Ga_xZn_{1-x}O$ nanoparticles with x = 0, 0.01, and 0.02 were synthesized to investigate the effect of Ga doping on the crystalline structure and thermoelectric properties of ZnO.

Although the abovementioned studies improved the thermoelectric performance of Ga-doped ZnO synthesized using solid-state reaction methods, they ignored the issue of environmental sustainability. In

Cite this article : Nguyen N H, Doan U T T, Hoang D V, Nguyen T H, Vo T Q, Tran V C, Pham A T T. **Thermo- electric properties of Ga-doped ZnO produced via a green synthesis method**. *VNUHCM J. Sci. Technol. Dev.* 2026; 29(1): 3919-3925.
This article was published during the journal title transition period from Science & Technology Development Journal 2026 (ISSN: 1859-0128) to VNUHCM Journal of Science and Technology Development; new ISSN pending assignment.

addition to optimizing material properties, environmental protection has become a pressing concern. Hence, there is a growing emphasis on environmentally friendly synthesis processes that avoid the use of toxic chemicals. One effective approach is to replace hazardous organic solvents with plant extracts and distilled water. Recent studies have demonstrated successful syntheses of nanostructured ZnO using natural extracts from *Morinda citrifolia* leaves[5], *Phoenix roebelenii* leaves[6], jujube fruit[7], orange peel[8], and potato peel[9]. Overall, these green synthesis methods offer several advantages over conventional chemical and physical methods, including eco-friendliness, procedural simplicity, low cost, ease of producing nanomaterials, and the potential for scalability for commercial production.

Here, orange peel extract was used as a stabilizing agent for the synthesis of Ga-doped ZnO nanoparticles (NPs) for thermoelectric applications. The extract was derived from discarded orange peels generated during juice production. Previous studies have shown that orange peels are rich in phenolic acids, flavonoids, and limonoids, which possess strong antioxidant and antibacterial properties, making them suitable stabilizers for ZnO NPs[10,11]. Thus, this study provides a sustainable approach for the synthesis of Ga-doped ZnO NPs and systematically explores their structural and thermoelectric properties.

MATERIALS AND METHODS

The orange peel extract was prepared by infusing dried orange peel powder in deionized (DI) water at a ratio of 1 gram to 50 mL of DI water. Initially, a metal salt mixture consisting of $Zn(NO_3)_2{\cdot}6H_2O$ (Thermo Scientific, 98%) and $Ga(NO_3)_3{\cdot}mH_2O$ (Sigma-Aldrich, 99.9%) was weighed to corresponding Ga doping contents of 0, 1, and 2 at.%. The orange peel extract was then added to the mixture and magnetically stirred at 500 rpm for 1 h. Subsequently, the solution was incubated at 80 °C for 1 h and dried at 350 °C. The resulting dried product was calcined at 850 °C for 1 h to obtain $Ga_xZn_{1-x}O$ NPs with x = 0, 0.01, and 0.02[8,12,13]. The samples for analyzing properties were pressed into circular pellets, which were sintered at 1000 °C for 1 h under a nitrogen atmosphere. After sintering, the surfaces and edges of the pellets were polished before analysis. The $Ga_xZn_{1-x}O$ samples with x = 0, 0.01, and 0.02 are referred to as ZnO, GZO-1, and GZO-2, respectively.

The crystalline structure was determined using X-ray diffraction (XRD, Bruker D8-Advance), with Cu-Ka radiation (λ = 0.15406 nm) at 40 kV and 30 mA. The morphology, elemental content, and distribution

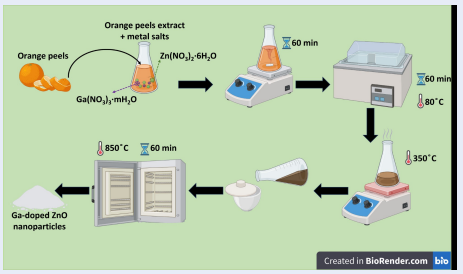

Figure 1: Schematic diagram of the green synthesis of $Ga_xZn_{1-x}O$ with x = 0, 0.01, and 0.02.

of the samples were determined using scanning electron microscopy (SEM, JSM-IT200, JEOL) at 10 kV. The carrier concentration and mobility were obtained from Hall effect-based measurements at room temperature (HMS3000, Ecopia) with a magnetic field of 0.55 T. The temperature-dependent thermoelectric properties, including electrical conductivity (σ), Seebeck coefficient (S), and power factor (PF), were determined using a Linseis LSR-3 system under a helium atmosphere from room temperature to 800 °C for two cycles. The thermal conductivity (κ) was measured using a laser flash method (Linseis, LFA500/1000) under an argon atmosphere from room temperature to 800 °C.

RESULTS AND DISCUSSION

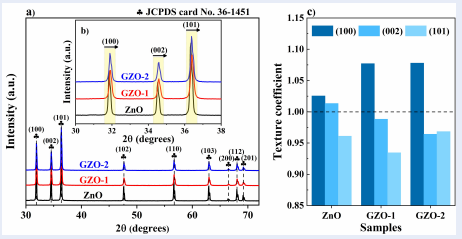

Figure 2: a) XRD patterns; b) enlarged XRD patterns in a 2θ range from 30° to 38° for the ZnO, GZO-1, and GZO-2 samples; c) texture coefficients corresponding to the (100), (002), and (101) planes of the samples.

All samples exhibited characteristic diffraction peaks of wurtzite-structured ZnO, as indicated by JCPDS card No. 36-1451 (Figure 2a). No peaks corresponding to Ga_2O_3 or the secondary spinel phase $Ga_2Zn_9O_{12}$ were found in the overall XRD patterns (Figure 2a)[14]. However, in the enlarged XRD patterns, a slight shift of the diffraction peaks toward higher angles was observed for the GZO-1 and GZO-2

samples within a 2 range of 30°–38° (Figure 2b). This shift was attributed to the difference in ionic radius between Zn^{2+} (0.074 nm) and Ga^{3+} (0.062 nm) [15]. This result suggests that Ga was incorporated into the ZnO crystal lattice as a dopant rather than forming a separate Ga-related phase [16].

Several parameters were calculated to evaluate the differences among the ZnO, GZO-1, and GZO-2 samples (Figure 2c and Table 1). First, the texture coefficient (TC) was calculated based on the (100), (002), and (101) planes to determine the preferred crystal growth orientation in the samples. Equation (1) was used to obtain the TC values for these three planes:

$$TC_{(hkl)} = \frac{I_m(hkl)}{I_o(hkl)} \left\{ \frac{1}{n} \sum_1^n \frac{I_m(hkl)}{I_o(hkl)} \right\}^{-1} \quad (1)$$

where I_m(hkl) and I_o(hkl) represent the measured intensity and the standard intensity of the ZnO peaks from JCPDS card No. 36-1451, respectively, and n (n = 3) is the number of diffraction planes considered. As shown in Figure 2c, the TC values for the (100) plane were greater than 1 for all samples, indicating a preferred crystal growth orientation along this plane. For the ZnO sample, the TC value of the (002) plane was approximately 1, suggesting a random orientation. However, the TC of the (101) plane was less than 1, implying a suppressed growth along this plane, despite the (002) peak exhibiting the highest intensity. By contrast, for both Ga-doped ZnO samples, the TC values of the (002) and (101) planes were further reduced and fell below 1, indicating restricted crystal growth in these directions. In other words, Ga-doped ZnO mainly grew along the (100) plane, while growth was suppressed along the other planes.

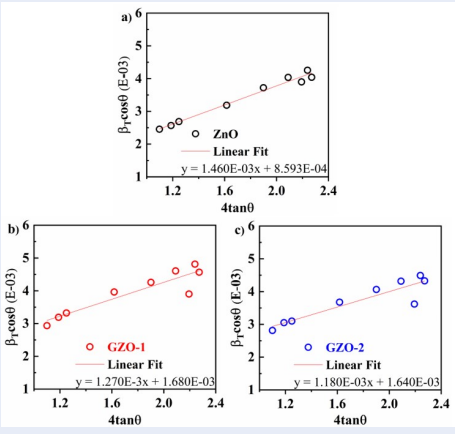

Figure 3: Williamson–Hall (W–H) plots of the samples: a) ZnO; b) GZO-1; c) GZO-2.

Moreover, the mean crystallite size (D) was estimated from the XRD patterns using both the Scherrer equation and the Williamson–Hall (W–H) method. In the Scherrer equation (Equation (2)), the mean crystallite size was calculated based on the three diffraction peaks corresponding to the (100), (002), and (101) planes:

$$D = \frac{k\lambda}{\beta \cos\theta} \quad (2)$$

where k is the constant (k = 0.9), λ represents the X-ray wavelength (λ = 0.15406 nm), (radians) stands for the full width at half maximum of the diffraction peak, and (radians) denotes the Bragg angle. Table 1 presents the calculated mean crystallite sizes corresponding to the three diffraction planes for each sample.

In contrast to the Scherrer equation, the W–H method assumes that both the crystallite size and the intrinsic microstrain in the crystal lattice influence the total broadening of the diffraction peaks [17]:

$$\beta_{hkl} = \beta_{size} + \beta_{strain} \quad (3)$$

Assuming the strain is uniformly distributed in all directions, the peak broadening caused by the microstrain can be expressed as:

$$\beta_{strain} = 4\varepsilon \tan\theta \quad (4)$$

Combining Equations (2) and (4), the total broadening can be expressed as:

$$\beta_{hkl} = \frac{k\lambda}{D\cos\theta} + 4\varepsilon \tan\theta \quad (5)$$

Rearranging Equation (5), we obtain:

$$\beta_{hkl} \cos\theta = \frac{k\lambda}{D} + 4\varepsilon \tan\theta \quad (6)$$

Figure 3 presents the W–H plots constructed with the x-axis as and the y-axis as, based on the diffraction peak data obtained from Figure 2a. Following linear fitting, the crystallite size was determined from the y-intercept and the microstrain was obtained from the slope. The corresponding results are summarized in Table 1.

The ZnO sample exhibited the largest crystallite size: ~54 nm according to the Scherrer equation and ~161 nm by the W–H method. By contrast, doping with Ga resulted in smaller mean crystallite sizes. GZO-1 exhibited a crystallite size of ~44 nm (Scherrer) and ~82 nm (W–H), while GZO-2 showed ~46 nm (Scherrer) and ~84 nm (W–H). This reduction in crystallite size can be attributed to the presence of Ga in the ZnO lattice, which likely increased the number of nuclei during the nucleation process, leading to more crystallites with smaller sizes [18]. In addition, the microstrain values were positive, indicating tensile strain. The strain decreased with increasing Ga doping concentration, from 1.46 x 10^{-3} (ZnO) to 1.27 x 10^{-3} (GZO-1), and further to 1.18 x 10^{-3} (GZO-2). Taha et al. [19] reported similar results in their study of Ga-doped ZnO NPs. When Ga^{3+} substitutes for Zn^{2+} in the lattice, it causes a compressed lattice because of its smaller ionic radius, reducing the microstrain. Furthermore, the crystallite sizes measured by the W–H

Table 1: Calculated crystallite sizes, lattice parameters, and unit cell volumes of the ZnO, GZO-1, and GZO-2 samples.

Sample	Crytallite size (nm)		Strain (10^{-3})	Lattice parameters		
	$D_{Scherrer}$	D_{W-H}		a (Å)	c (Å)	V (Å^3)
ZnO	54.01	161.36	1.46	3.240	5.189	47.168
GZO-1	44.10	82.53	1.27	3.234	5.181	46.925
GZO-2	46.44	84.55	1.18	3.235	5.182	46.962

method were consistently larger than those obtained by the Scherrer equation. This discrepancy is due to the fundamental assumptions of the two methods: the Scherrer equation considers only size-induced peak broadening, whereas the W–H method accounts for both crystallite size and microstrain effects. Due to the difference in ionic radius between Zn^{2+} (0.074 nm) and Ga^{3+} (0.062 nm), Ga incorporation into the ZnO lattice caused lattice compression, inducing microstrain in the samples (20). Therefore, the W–H method can be considered more reliable. However, the measured microstrain values were small; thus, the impact of strain on peak broadening might be minor, and the differences between these methods need to be further clarified in future investigations.

ZnO exhibits a hexagonal wurtzite structure; therefore, the lattice parameters a, c, and the unit cell volume V were determined using the following equations:

$$\frac{1}{d_{hkl}^2} = \frac{4}{3}\left(\frac{h^2+hk+k^2}{a^2}\right) + \frac{l^2}{c^2} \quad (7)$$

$$V = 0.866 \times a^2 \times c \quad (8)$$

The interplanar spacing d_{hkl} was calculated using Bragg's equation:

$$2d_{hkl}\sin\theta = n\lambda \quad (9)$$

The lattice parameters a and c were calculated from the (100) and (002) diffraction peaks, using the following formulas:

$$a = \frac{\lambda}{\sqrt{3}\sin\theta_{(100)}} \quad (10)$$

$$c = \frac{\lambda}{\sin\theta_{(002)}} \quad (11)$$

Table 1 summarizes the values of the lattice parameters a, c, and the unit cell volume V for the samples. Compared to ZnO, both GZO-1 and GZO-2 showed slight reductions in a and c, resulting in a corresponding decrease in V. As previously mentioned, this phenomenon can be attributed to the lattice contraction caused by the substitution of Ga^{3+} for Zn^{2+} in the ZnO lattice. Therefore, the lattice parameters decreased accordingly. However, the magnitude of the changes was small, indicating that the Ga doping concentrations employed in this study did not induce substantial lattice distortion.

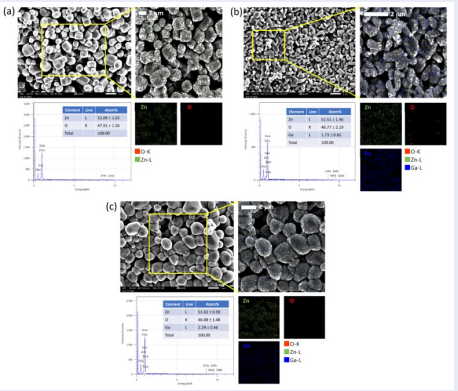

Figure 4: SEM images, EDXspectra, and elemental mapping of the samples after sintering: a) ZnO; b) GZO-1;c) GZO-2.

The SEM images of the samples (Figure 4) showed that both the ZnO and GZO-1 samples consisted of hexagonal prism-shaped particles; however, ZnO exhibited more uniform particles compared with GZO-1. On the other hand, GZO-2 displayed polyhedral particles with rounded edges, giving them a nearly spherical appearance. As shown in the SEM images, the ZnO sample exhibited the largest particle size, while Ga doping markedly suppressed particle growth. GZO-1 exhibited the smallest particle size, while the grain size of GZO-2 slightly increased, approaching that of pure ZnO. Overall, Ga doping hindered grain growth, resulting in the GZO samples having smaller particles than those of ZnO. This effect was attributed to the diffusion of Ga atoms into the ZnO lattice, which promoted nucleation and reduced the particle growth rate [18]. In addition, by correlating the crystallite size results from the Scherrer equation and the W–H method in the XRD analysis with those of SEM, we found that the crystallite size estimated by the W–H method was closer to the particle size from the SEM images. Therefore, the W–H method provided a more reliable estimate of the crystallite size in the samples. The quantitative EDX analysis revealed that the atomic percentage of Ga increased progressively with

the Ga doping ratio (Figure 4). Furthermore, the EDX mapping results revealed a uniform distribution of Ga dopants across the examined regions, without any evidence of secondary phase segregation, demonstrating that Ga atoms were incorporated into the ZnO lattice. Figure 5 presents the variation of electrical conductivity (σ) with temperature. The ZnO sample exhibited minimal conductivity of ~2.2 S/cm at 1068 K, which is likely due to the low carrier concentration of ZnO, as reported in numerous studies. However, the values of the Ga-doped ZnO samples increased significantly with increasing Ga concentration. At 1068 K, GZO-1 achieved ~21 S/cm (over nine times higher than that of ZnO), while GZO-2 reached ~64.3 S/cm (approximately 29 times higher than that of ZnO). This enhancement in conductivity could be attributed to the substitution of Zn^{2+} ions with Ga^{3+} ions in the crystal lattice. These ions released free electrons and increased the carrier concentration in the GZO-1 and GZO-2 samples. Additionally, XRD analysis indicated a decrease in microstrain with increasing Ga doping concentration. Lower microstrain may thus contribute to enhanced carrier mobility, improving electrical conductivity. Hong et al. reported similar findings, where increasing microstrain in Al-doped ZnO thin films with varying Al contents markedly reduced carrier mobility and generated a saturation of electrical conductivity.

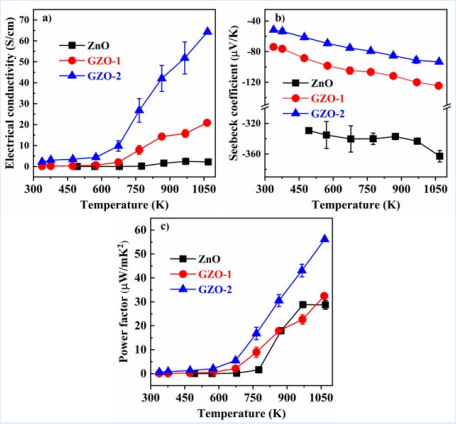

Figure 5: Temperature-dependentthermoelectric properties: a) electrical conductivity (σ); b) Seebeckcoefficient (S); c) power factor (PF) for ZnO, GZO-1, and GZO-2.

However, the Hall effect measurement results revealed that the carrier mobility (μ_H) of the samples exhibited an opposite trend compared with the initial assumption: the lowest μ_H corresponded to GZO-1 (8.24 cm^2/Vs), followed by GZO-2 (5.63 cm^2/Vs), whereas the highest μ_H corresponded to ZnO (25.32 cm^2/Vs). To explain this discrepancy, the fact that the carrier concentration (n_e) of the samples increased progressively with Ga doping should be considered. In particular, n_e in the Ga-doped ZnO samples increased by several orders of magnitude (from 3.7 x 10^{16} cm^{-3} for ZnO to 1.2 x 10^{18} cm^{-3} for GZO-1 and 5.1 x 10^{18} cm^{-3} for GZO-2), which, in turn, strongly enhanced ionized impurity scattering. In addition, the SEM images (Figure 4) revealed that the particle sizes of both Ga-doped ZnO samples were much smaller than those of ZnO, further increasing grain boundary scattering. The combined effects of these scattering mechanisms outweighed the influence of reduced microstrain, markedly decreasing μ_H. Thus, although microstrain may influence carrier mobility, as reported by Hong et al., conductivity enhancement in this case was predominantly governed by the increase in carrier concentration.

Because ZnO is an n-type semiconductor, all three samples exhibited negative S values (Figure 5b). The ZnO sample displayed large S values throughout the measured temperature range because of its low carrier concentration: S spanned from −330 to −363 μV/K in the range of 492–1068 K. By contrast, the Ga-doped ZnO samples exhibited notably lower S values than those of ZnO. The GZO-1 sample showed an S value of −125 μV/K at 1068 K, while GZO-2 reached only −93 μV/K at the same temperature.

The power factor (PF = σS^2) was calculated based on the measured σ and S data at each temperature, and is presented in Figure 5c. Owing to its high S value, the ZnO sample exhibited a PF of ~29 $\mu W/mK^2$ at 1068 K, which was not significantly different from that of GZO-1 (~32 $\mu W/mK^2$), despite the much higher of the latter. However, GZO-2, which possessed the highest along with a moderate S, achieved the highest PF of approximately 56 $\mu W/mK^2$ at 1068 K, about 1.9 times higher than that of pure ZnO, demonstrating the potential of Ga doping for enhancing electrical properties.

Moreover, doping could markedly affect the thermal properties of the material. **Figure 6**a presents the temperature-dependent thermal conductivity (κ) of ZnO and the Ga-doped ZnO samples to gain further insights into their thermal behavior. The ZnO sample exhibited a high κ value (~14 W/mK) at room temperature. By contrast, the κ of the samples decreased markedly when Ga was added, with GZO-1 reaching 6.8 W/mK and GZO-2 reaching 4.1 W/mK. As the temperature increased to 1068 K, the κ of ZnO decreased to ~4 W/mK, while the κ values of GZO-1 and GZO-2 showed slight reductions, reaching 2.8 W/mK

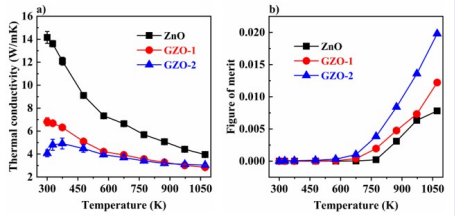

Figure 6: Temperature-dependent a) thermal conductivity (κ) and b) figure of merit (ZT) of ZnO, GZO-1, and GZO-2.

and 3 W/mK, respectively. This decrease could be attributed to the difference in atomic mass between Zn and Ga, which enhanced phonon scattering and reduced thermal conductivity. Notably, GZO-1 exhibited the lowest κ at 1068 K. This result is consistent with the SEM images (Figure 4), which show that GZO-1 had the smallest mean particle size. The nano-sized particles increased the grain boundary density, enhancing phonon-boundary scattering and further contributing to the reduction in thermal conductivity.

The thermoelectric performance of the samples was evaluated by the figure of merit (ZT), defined as ZT = PFxT/κ (Figure 6b). Owing to its improved electrical properties and reduced thermal conductivity, GZO-2 exhibited the best thermoelectric performance among the samples. In particular, GZO-2 achieved a ZT value of 0.02, which was 2.5 times higher than that of pristine ZnO at 1072 K, demonstrating the potential of Ga doping for enhancing thermoelectric performance. Table 2 summarizes several reports on bulk Ga-doped ZnO, including the synthesis methods, fabrication processes, power factors, and ZT of the samples, for comparison with the results of this study. Although the obtained values were lower than those reported in previous studies, they demonstrate the potential of green synthesis for preparing Ga-doped ZnO thermoelectric materials. The proposed approach represents an environmentally friendly and low-cost alternative to conventional solid-state reaction methods, offering a valuable direction for future research.

CONCLUSIONS

Ga-doped ZnO nanoparticles were obtained via a green synthesis method using orange peel extract. Doping Ga into the ZnO crystal lattice enhanced electrical conductivity through two simultaneous effects. First, the substitution of Zn^{2+} with Ga^{3+} ions released additional free electrons, increasing the carrier concentration. Second, XRD analysis revealed a reduction in microstrain with increasing Ga content, which might contribute to improved carrier mobility. The combination of higher carrier concentration and enhanced mobility was the primary factor responsible for the substantial increase in electrical conductivity observed in the GZO samples compared to pure ZnO. In particular, GZO-2 achieved the highest power factor of approximately 56 μW/mK^2 at 1068 K, nearly twofold higher than that of the ZnO sample. Simultaneously, the reduction in particle size— confirmed by the SEM images—enhanced phonon-boundary scattering, decreasing thermal conductivity. As a result of the synergistic effect of a high power factor and low thermal conductivity, the figure of merit of GZO-2 was 2.5 times higher than that of ZnO.

COMPETING INTERESTS

The authors declare that they have no competing interests.

AUTHORS' CONTRIBUTIONS

N.H. Nguyen: Data curation, Investigation, Formal analysis, Writing – original draft. U.T.T. Doan: Data curation, Investigation. D.V. Hoang: Data curation. T.H. Nguyen: Data curation. T.Q. Vo: Data curation. V.C. Tran: Resources, Methodology, Validation, Supervision, Funding acquisition. A.T.T. Pham: Conceptualization, Supervision, Data curation, Writing – review & editing.

ACKNOWLEDGEMENTS

This research is funded by Vietnam National University, Ho Chi Minh City (VNU-HCM) under grant number B2025-18-06.

REFERENCES

1. Sulaiman S, Izman S, Uday MB, Omar MF. Review on grain size effects on thermal conductivity in ZnO thermoelectric materials. RSC Adv. 2022;12(9):5428–38. Available from: https://doi.org/10.1039/d1ra06133j.
2. Jung K, Lee KH, Seo W, Choi S, Jung K, Lee KH, et al. An enhancement of a thermoelectric power factor in a Ga-doped ZnO system: A chemical compression by enlarged Ga solubility. Appl Phys Lett. 2012;2014(253902):2010–4. Available from: https://doi.org/10.1063/1.4729560.
3. Guilmeau E, Díaz-Chao P, Lebedev OI, ReA, Schäfer MC, Delorme F, et al. Inversion Boundaries and Phonon Scattering in Ga:ZnO Thermoelectric Compounds. Inorg Chem. 2017;56(1):480–7. Available from: https://doi.org/10.1021/acs.inorgchem.6b02354.
4. Shreema K, Mathammal R, Kalaiselvi V, Vijayakumar S, Selvakumar K, Senthil K. Green synthesis of silver doped zinc oxide nanoparticles using fresh leaf extract Morinda citrifoliaand its antioxidant potential. Mater Today Proc. 2021;47:2126–31. Available from: https://doi.org/10.1016/j.matpr.2021.04.627.

Table 2: Comparison of synthesis methods, fabrication processes, power factor (PF), and figure of merit (ZT) of bulk Ga-doped ZnO samples from several studies and this work.

Materials	Synthesis method	Fabrication process	PF (μW/mK^2)	ZT	Ref.
$Zn_{0.985}Ga_{0.015}O$	Ball milling	Sintering at 1373 K in N_2, hot-pressing at 1273 K in vacuum	1250 (at 1273 K)	0.25 (at 1273 K)	2
$Zn_{0.98}Ga_{0.02}O$	Ball milling	Sintering at 1673 K in air	918 (at 1050 K)	–	3
$Zn_{0.995}Ga_{0.005}O$	Ball milling	Sintering at 1673 K in air	700 (at 1000 K)	0.09 (at 1000 K)	4
$Zn_{0.995}Ga_{0.005}O$	Ball milling	Calcining at 1373 K, hot-pressing at 1423 K in vacuum	990 (at 1046 K)	0.22 (at 1046 K)	
$Zn_{0.98}Ga_{0.02}O$	Green synthesis using orange peel extract	Sintering at 1273 K in N_2 atmosphere	56 (at 1068 K)	0.02 (at 1068 K)	This work

5. Aldeen TS, Mohamed HEA, Maaza M. ZnO nanoparticles prepared via a green synthesis approach: physical properties, photocatalytic and antibacterial activity. J Phys Chem Solids. 2022;160. Available from: https://doi.org/10.1016/j.jpcs.2021.110313.
6. Golmohammadi M, Honarmand M, Ghanbari S. A green approach to synthesis of ZnO nanoparticles using jujube fruit extract and their application in photocatalytic degradation of organic dyes. Spectrochim Acta A Mol Biomol Spectrosc. 2020;229. Available from: https://doi.org/10.1016/j.saa.2019.117961.
7. Thi TUD, Nguyen TT, Thi YD, Thi KHT, Phan BT, Pham KN. Green synthesis of ZnO nanoparticles using orange fruit peel extract for antibacterial activities. RSC Adv. 2020;10(40):23899–907. Available from: https://doi.org/10.1039/d0ra04926c.
8. Alharthi FA, Alghamdi AA, Al-Zaqri N, Alanazi HS, Alsyahi AA, Marghany AE, et al. Facile one-pot green synthesis of Ag-ZnO Nanocomposites using potato peeland their Ag concentration dependent photocatalytic properties. Sci Rep. 2020;10(1):20229. Available from: https://doi.org/10.1038/s41598-020-77426-y.
9. Gorinstein S, Martín-Belloso O, Park YS, Haruenkit R, Lojek A, ÍM, et al. Comparison of some biochemical characteristics of different citrus fruits. Food Chem. 2001;74(3):309–15. Available from: https://doi.org/10.1016/S0308-8146(01)00157-1.
10. Singh B, Singh JP, Kaur A, Singh N. Phenolic composition, antioxidant potential and health benefits of citrus peel. Food Res Int. 2020;132. Available from: https://doi.org/10.1016/j.foodres.2020.109114.
11. Pham AT, Luu TA, Pham NK, Ta HK, Nguyen TH, Van HD, et al. Multi-scale defects in ZnO thermoelectric ceramic materials co-doped with In and Ga. Ceram Int. 2020;46(8):10748–58. Available from: https://doi.org/10.1016/j.ceramint.2020.01.084.
12. An HR, Baek SH, Park IK, Ahn HJ. Electrical and optical properties of Al-doped ZnO films deposited by atomic layer deposition. Korean J Mater Res. 2013;23(8):469–75. Available from: https://doi.org/10.3740/MRSK.2013.23.8.469.
13. Lim SK, Hong SH, Hwang SH, Kim S, Park H. Characterization of Ga-doped ZnO Nanorods Synthesized via Microemulsion Method. J Mater Sci Technol. 2013;29(1):39–43. Available from: https://doi.org/10.1016/j.jmst.2012.11.005.
14. Nath D, Singh F, Das R. X-ray diffraction analysis by Williamson-Hall, Halder-Wagner and size-strain plot methods of CdSe nanoparticles- a comparative study. Mater Chem Phys. 2020;239. Available from: https://doi.org/10.1016/j.matchemphys.2019.122021.
15. Tsay CY, Wu CW, Lei CM, Chen FS, Lin CK. Microstructural and optical properties of Ga-doped ZnO semiconductor thin films prepared by sol-gel process. Thin Solid Films. 2010;519(5):1516–20. Available from: https://doi.org/10.1016/j.tsf.2010.08.170.
16. Taha I, Abdulhamid ZM, Straubinger R, Emwas AH, Polychronopoulou K, Anjum DH. Ga-doped ZnO nanoparticles for enhanced CO2 gas sensing applications. Sci Rep. 2024;14(1):29712. Available from: https://doi.org/10.1038/s41598-024-81279-0.
17. Jood P, Mehta RJ, Zhang Y, Peleckis G, Wang X, Siegel RW, et al. Al-doped zinc oxide nanocomposites with enhanced thermoelectric properties. Nano Lett. 2011;11(10):4337–42. Available from: https://doi.org/10.1021/nl202439h.
18. Acharya S, Yu B, Hwang J, Kim J, Kim W. High Thermoelectric Performance of ZnO by Coherent Phonon Scattering and Optimized Charge Transport. Adv Funct Mater. 2021;31(43). Available from: https://doi.org/10.1002/adfm.202105008.
19. Hong MH, Choi H, Shim D. Study of the effect of stress/strain of mesoporous Al-doped ZnO thin films on thermoelectric properties. Solid State Sci. 2018;82:84–91. Available from: https://doi.org/10.1016/j.solidstatesciences.2018.05.010.